Catalytic Functions of Mo/Ni/MgO in the Synthesis of Thin Carbon Nanotubes

Ling-Ping Zhou,[†] Keishin Ohta,[‡] Keiji Kuroda, Ni Lei, Kiyoto Matsuishi, Lizhen Gao,[§] Taketoshi Matsumoto,[||] and Junji Nakamura*

Materials Science, Graduate School of Pure and Applied Sciences, University of Tsukuba, Tennoudai 1-1-1, Tsukuba, Ibaraki 305-8573, Japan

Received: October 15, 2004; In Final Form: December 8, 2004

The functions and structures of Mo/Ni/MgO catalysts in the synthesis of carbon nanotubes (CNTs) have been investigated by transmission electron microscopy (TEM), X-ray diffraction (XRD), X-ray photoelectron spectroscopy (XPS), and Raman spectroscopy. Thin 2−5-walled CNTs with high purities (over 90%) have been successfully synthesized by catalytic decomposition of CH_4 over Mo/Ni/MgO catalysts at 1073 K. It has been found that the yield of CNTs as well as the outer diameter or thickness correlates well with the contents of these three elements. The three components Mo, Ni, and MgO are all necessary to synthesize the thin CNTs at high yields since no catalytic activity was observed for CNT synthesis when one of these components was not present. The outer diameter of the CNTs increases from 4 to 13 nm and the thickness of graphene layers also increases with increasing Mo content at a fixed Ni content, while the inner diameter stays at 2−3 nm regardless of their contents. Furthermore, the average outer diameter is in good agreement with the average particle size of metal catalyst. That is, the thickness or the outer diameter can be controlled by selecting the composition of the Mo/Ni/MgO catalysts. XRD analyses have shown that Mo and Ni form a Mo−Ni alloy before CNT synthesis, while the Mo−Ni alloy phase is separated into Mo carbide and Ni. These alloy particles are supported on MgO cubic particles 15−20 nm in width. It has been found that only small Mo−Ni alloy particles 2−16 nm in size catalyze CNT synthesis, with larger particles over 15 nm exhibiting no activity. Mo carbide and Ni should play different roles in the synthesis of the thin CNTs, in which Ni is responsible for the dissociation of CH_4 into carbon and Mo_2C works as a carbon reservoir.

1. Introduction

Since the discovery of single-walled carbon nanotubes (SWCNTs) by Iijima,[1] carbon nanotubes (CNTs) have attracted great interest as a new carbon material, both in fundamental science and in industrial applications.[2] Catalytic chemical vapor deposition (CCVD) has been recognized as the most practical synthetic method for carbon nanotubes, with low cost and high yield. Catalyst components usually include transient metals such as Fe, Co, and Ni, and hydrocarbons or CO is used as the feedstock for the CNT synthesis. The morphology and quality of CNTs vary depending on the catalysts, carbon sources, temperatures, flow rates, and feedstock pressures. So far, the controlled growth of CNTs with respect to their diameter and the number of layers has been a bottleneck for applications of these advanced materials. Understanding the growth mechanism and the kinetics is crucial for research in CNT synthesis. The CNT growth mechanism includes several elementary steps taking place on the surface and bulk of the catalysts, such as dissociation of CO or hydrocarbons into carbon on the catalyst surfaces, migration of carbon into the bulk of the catalysts, segregation of carbon onto the surfaces, and formation of graphene sheets.

It has been reported that not only does Mo by itself has catalytic reactivity of SWCNT formation[3] but also the addition of Mo into Fe- or Co-based catalysts promotes thin CNT synthesis. Thin multiwalled carbon nanotubes (MWCNTs) and SWCNTs have been synthesized over Mo/Co/Mg,[4,5] Mo/Co/SiO_2,[6] Mo/Fe/Al_2O_3 (aerogel),[7] Mo/Fe/SiO_2−Al_2O_3,[8] and Mo/Fe/Al_2O_3.[9] For example, addition of Mo to Co/MgO increased the yield of SWCNTs by an order of magnitude,[4] where MWCNTs were formed beyond an optimal Mo amount. The bimetallic catalysts including Mo are promising for the synthesis of both SWCNTs and MWCNTs in a controlled manner. However, it is still unknown why the addition of Mo changes the catalytic nature of Co or Fe catalysts.[5]

Among various catalyst supports, MgO possesses the advantage of being removed easily from the CNT products by acids. It is also well-known that the sol−gel method is available for preparing highly dispersed metal particles supported on cubic MgO particles.

In this study, we find Mo/Ni/MgO catalysts for synthesizing thin MWCNTs with control of the average outer diameter and average thickness of walls, and we report on the state of the catalysts during the CNT synthesis and on the catalytic roles of Mo, Ni, and MgO.

2. Experimental Section

2.1. Catalyst Preparation. $(NH_4)_6Mo_7O_{24}\cdot 4H_2O$, $Ni(NO_3)_2\cdot 6H_2O$ and $Mg(NO_3)_2\cdot 6H_2O$ (Wako Pure Chemical Industries, Ltd.) were mixed stoichiometrically and ground thoroughly, followed by addition of 1 g of citric acid and several drops of deionized water. The mixture was ground again to make a uniform pastelike sample and calcined at 823 K in air for 20 min. The foam material obtained was used for CNT synthesis.

* Corresponding author: tel and fax +81-29-853-5279; e-mail nakamura@ims.tsukuba.ac.jp.

[†] Present address: The Research Institute of Petroleum Processing, Xueyuan Road 18, Beijing 100083, P. R. China.

[‡] Present address: Microphase Ltd., Japan.

[§] Present address: Shenzhen University, China.

[||] Present address: Institute for Molecular Science, Japan.

10.1021/jp045284e CCC: $30.25 © 2005 American Chemical Society
Published on Web 02/19/2005

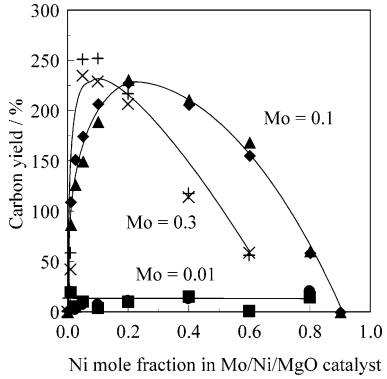

Figure 1. Carbon yield produced by decomposition of CH_4 at 1073 K for 1 h on Mo/Ni/MgO catalysts as a function of the Ni/MgO ratio: (■) $Mo_{0.01}Ni_xMg_{0.99-x}O$ (right boat), (●) $Mo_{0.01}Ni_xMg_{0.99-x}O$ (left boat), (▲) $Mo_{0.1}Ni_xMg_{0.9-x}O$ (right boat), (◆) $Mo_{0.1}Ni_xMg_{0.9-x}O$ (left boat), (+) $Mo_{0.3}Ni_xMg_{0.7-x}O$ (right boat), and (×) $Mo_{0.3}Ni_xMg_{0.7-x}O$ (left boat).

2.2. CNT Synthesis. CNTs were synthesized by the catalytic decomposition of methane diluted with nitrogen (4.93% CH_4, 96.07% N_2) at 1073 K over Mo/Ni/MgO catalysts. Decomposition of methane was carried out in a fixed-bed flow reactor made of a quartz tube (i.d. 2.5 cm, length 55 cm) laid on a horizontal furnace with a thermocouple in its central zone. Two quartz boats with 20 mg of catalyst each were placed in the central part of the reactor. The catalyst was heated to 923 K in N_2 (100 sccm) and then reduced for 1 h at 923 K with H_2 gas (H_2/N_2 = 60/100 v/v). Subsequently, the temperature was raised to 1073 K, and methane (144 sccm) was fed when the reaction temperature was stable. After 1 h of reaction, methane was switched to nitrogen (100 sccm) during cooling. Finally, the CNTs with the catalysts were collected from these two quartz boats.

The carbon yield of each boat was calculated as follows:

$$\text{carbon}_{\text{yield}} = \frac{W_{\text{products}} - W_{\text{catalysts}}}{W_{\text{catalysts}}} \times 100$$

where W_{products} denotes the total weight of carbon and catalyst after 1 h of reaction and and $W_{\text{catalysts}}$ is the weight of catalyst before reaction.

2.3. X-ray Diffraction. Powder X-ray diffraction (XRD) patterns of the catalysts were obtained with a Philips X′Pert MRD diffractometer by use of nickel-filtered Cu Kα radiation. Samples were pressed on a Si single-crystal plate. The patterns were recorded over $5° < 2\theta < 90°$.

3. Results and Discussion

3.1. CNT Synthesis by Mo/Ni/MgO Catalysts. *3.1.1. Effect of Mo and Ni Content on Carbon Yield.* The CNT synthesis was carried out by decomposition of CH_4 at 1073 K for 1 h. The yield of deposited carbon was measured by varying the content of Ni in the Mo/Ni/MgO catalysts in order to examine the effect of the catalyst composition on the activity of the catalysts. Figure 1 shows the carbon yield as a function of the Ni mole fraction at fixed Mo mole fractions of 0.01, 0.1, and 0.3 ($Mo_{0.01}Ni_xMg_{0.99-x}O$, $Mo_{0.1}Ni_xMg_{0.9-x}O$, and $Mo_{0.3}Ni_xMg_{0.7-x}O$). The purity of carbon nanotubes in the carbon deposit was estimated to be above 90% on the basis of the TEM observations as described later. The carbon yield was always low for catalysts with Mo = 0.01 or 0 at any Ni mole fractions. This indicates that Ni/MgO is inactive for carbon formation under the present reaction conditions.[10]

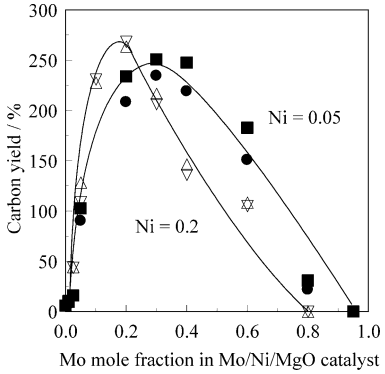

Figure 2. Carbon yield produced by decomposition of CH_4 at 1073 K for 1 h on Mo/Ni/MgO catalysts as a function of the Mo/MgO ratio: (■) $Mo_xNi_{0.05}Mg_{0.95-x}O$ (right boat), (●) $Mo_xNi_{0.05}Mg_{0.95-x}O$ (left boat), (△) $Mo_xNi_{0.2}Mg_{0.8-x}O$ (right boat), and (▽) $Mo_xNi_{0.2}Mg_{0.8-x}O$ (left boat).

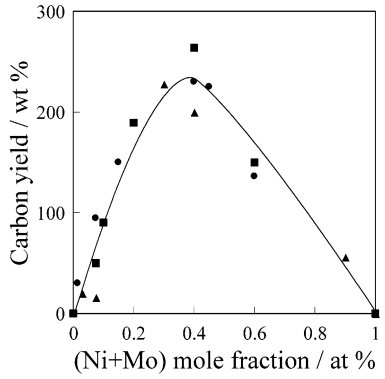

Figure 3. Carbon yield produced by decomposition of CH_4 at 1073 K for 1 h on Mo/Ni/MgO catalysts as a function of the metal fraction: (●) Mo/Ni = 2, (■) Mo/Ni = 1, and (▲) Mo/Ni = $^1/_2$.

It was also found that Mo/MgO catalysts showed no activity at all. However, addition of Ni to Mo/MgO drastically promoted the carbon yield as shown in Figure 1. That is, coexistence of Ni and Mo significantly promotes the formation of carbon. It is worth noting in Figure 1 that more Mo needs less Ni to obtain the highest carbon yields. The optimal sum of Mo and Ni mole fractions is 0.3−0.4.

The carbon yield decreased gradually at higher Ni mole fractions and no carbon was deposited in the absence of MgO. Thus, Ni, Mo, and MgO were all essential to produce the carbon deposit from CH_4 under the reaction conditions used.

We then changed the Mo content while fixing the Ni mole fraction in Mo/Ni/MgO catalysts. Figure 2 shows the carbon yield as a function of the Mo mole fraction at fixed fractions of Ni (0.05 and 0.2), that is, $Mo_xNi_{0.05}Mg_{0.95-x}O$ and $Mo_xNi_{0.20}Mg_{0.80-x}O$ catalysts. The carbon yield increased steeply with increasing Mo content at lower Mo contents (<0.2) and then decreased at higher Mo contents. The yield was zero when MgO was absent in the catalyst. We first assumed two possibilities for the decrease in the carbon yield at higher Mo (or Ni) mole fractions: one is the unbalanced content between Ni and Mo and the other is the requirement for the presence of MgO. To clarify these possibilities, we examined the carbon deposition over catalysts with a Mo/Ni molar ratio of 1:1 ($Mo_xNi_xMg_{1-2x}$) as shown in Figure 3. Again, without MgO the Mo_xNi_x catalyst showed no carbon deposits, indicating that an unbalanced Mo/Ni ratio is not the reason for the decrease in the carbon yield at higher metal fractions but that MgO is a crucial material for the CNT synthesis catalysts.

The decrease in carbon yield at higher total contents of Mo and Ni is thus ascribed to the decrease in MgO content. The

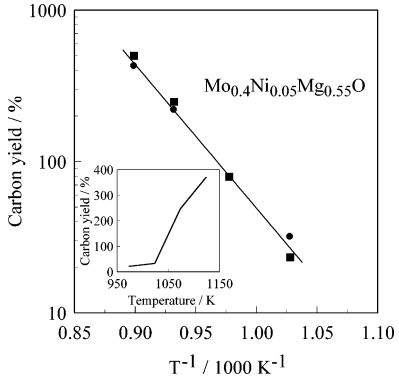

Figure 4. Arrhenius plot of the carbon yield on $Mo_{0.4}Ni_{0.05}Mg_{0.55}O$ catalyst: (■) right boat and (●) left boat. (Inset) Carbon yields for the right boat.

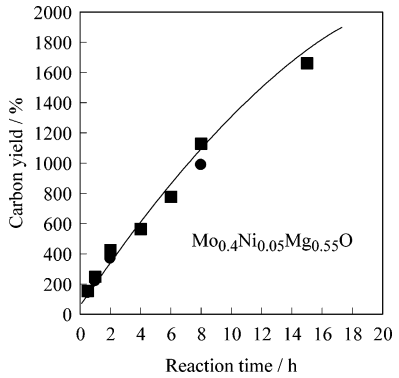

Figure 5. Relationship between reaction time and carbon yield on $Mo_{0.4}Ni_{0.05}Mg_{0.55}O$ catalyst at 1073 K: (■) right boat and (●) left boat.

catalyst particles composed of Mo and Ni will not be supported on MgO particles at lower contents of MgO, which leads to sintering of Mo and Ni metal particles. Note that the peak maxima in Figures 1−3 always seem to appear when the total mole fraction of Ni and Mo reaches 0.3−0.4. The decrease in the carbon yield above a total mole fraction of 0.4 can be thus explained by the larger particles of Mo and Ni being completely inactive for CNT synthesis under our reaction conditions. In other words, only small Mo and Ni particles supported on MgO show catalytic activity for CNT synthesis. The results shown above clearly indicate that the composition of the Mo/Ni/MgO catalysts sensitively controls the CNTs yield, because all three components are necessary for CNT synthesis.

3.1.2. Carbon Yield versus Reaction Temperature and Reaction Time. The effect of the reaction temperature on the carbon yield was examined for a $Mo_{0.4}Ni_{0.05}Mg_{0.55}$ catalyst. The carbon yields at 973, 1023, 1073, and 1123 K were 31.8, 78.7, 219.1, and 426.7 wt % for a reaction time of 1 h. Figure 4 shows the Arrhenius plot of the carbon yield. The activation energy was estimated to be 43.9 kcal/mol.

The lifetime of the catalyst for CNT production was studied for 16 h. The dependence of the carbon yield on the reaction time is plotted in Figure 5. The carbon yield increased almost linearly with reaction time, indicating no significant deactivation of the catalyst. Generally, in the CCVD method, CNTs grow by the tip mechanism on Ni catalysts, in which the Ni particles are present at the tip of the CNTs as an active site for growth. The results in Figure 5 imply that the catalyst particles are located at the tips of the tubes and are always exposed to the reactant CH_4, without being blocked by formed CNTs. On the basis of this phenomenon, it is expected that longer CNTs should be obtained with prolonged reaction times. Indeed, TEM observation showed that the CNTs synthesized for 8 h were much longer than those synthesized for 1 h.

3.2. Characterization of CNTs. *3.2.1. TEM of CNTs.* The carbon products obtained over $Mo_xNi_{0.05}Mg_{0.95-x}O$ catalysts with different Mo fractions were characterized by TEM. Figure 6a−d shows TEM images of as-grown carbon nanotubes synthesized from methane at 1073 K for 8 h. The purity of CNTs was roughly estimated to be over 90%, although it was difficult to determine by TEM whether the dark impurities were amorphous carbon or catalysts used for the synthesis. In the TEM

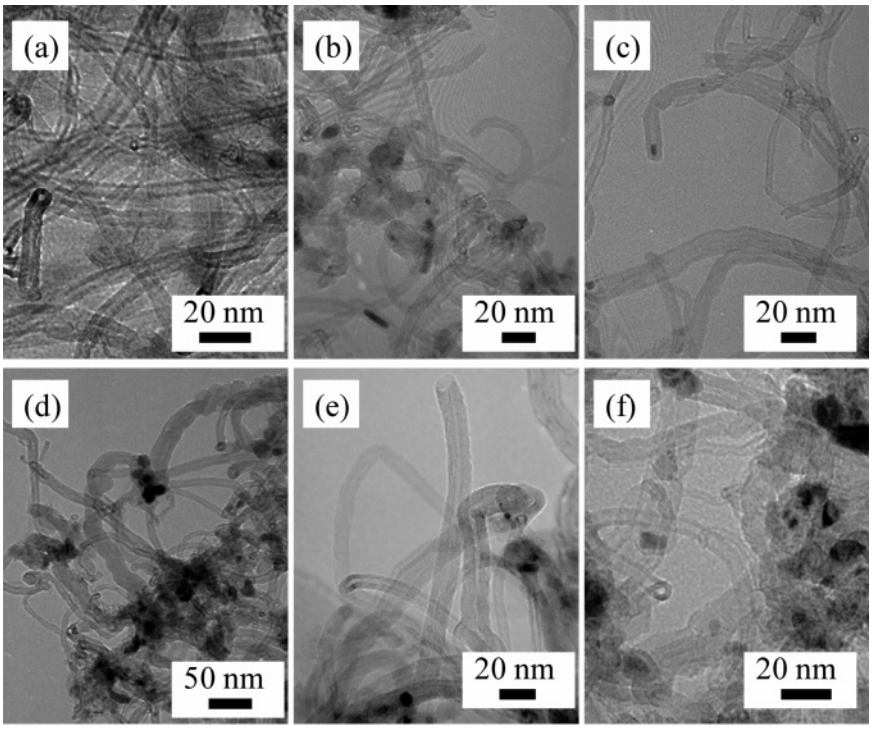

Figure 6. TEM images of as-grown carbon nanotubes produced by catalytic decomposition of CH_4 at 1073 K for 8 h over (a) $Mo_{0.025}Ni_{0.05}Mg_{0.925}$, (b) $Mo_{0.05}Ni_{0.05}Mg_{0.9}$, (c) $Mo_{0.1}Ni_{0.05}Mg_{0.85}$, (d) $Mo_{0.2}Ni_{0.05}Mg_{0.75}$, (e) $Mo_{0.4}Ni_{0.05}Mg_{0.55}$, and (f) $Mo_{0.6}Ni_{0.05}Mg_{0.35}$.

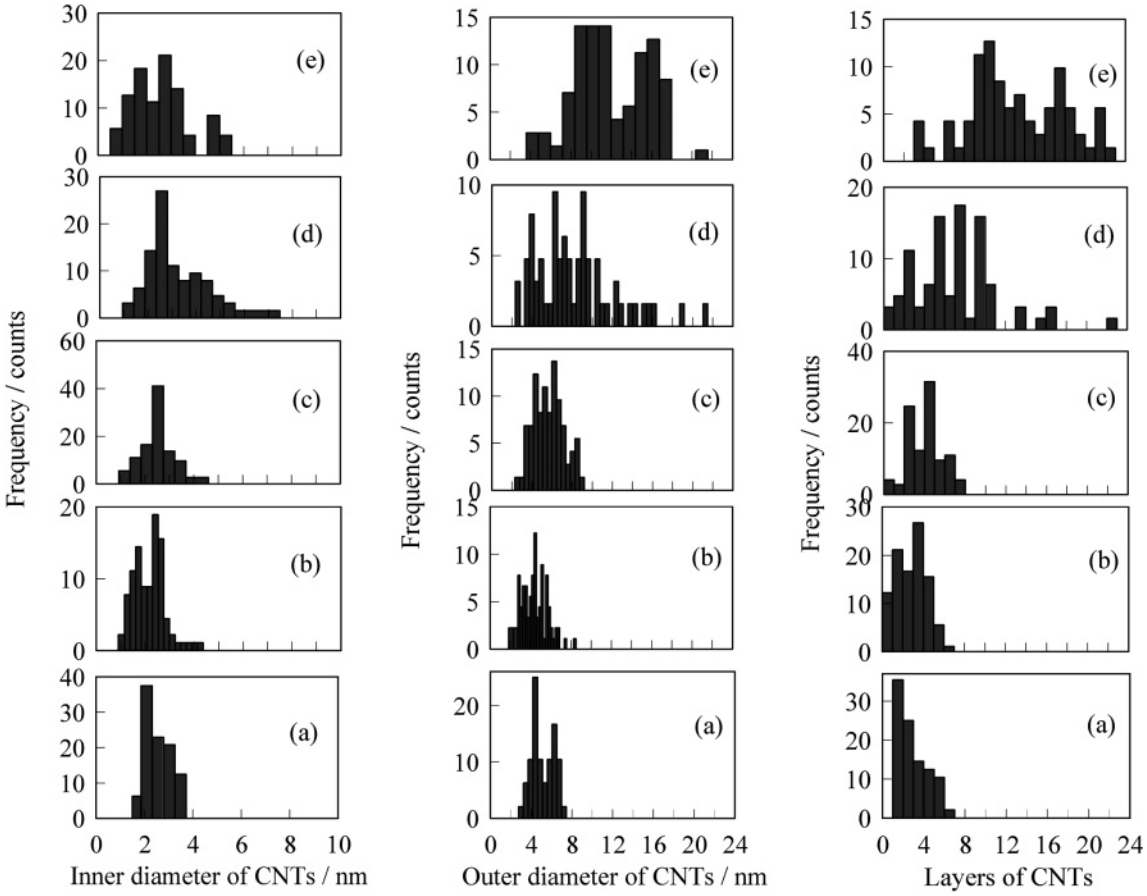

Figure 7. Size distribution histograms of CNTs synthesized over (a) $Mo_{0.025}Ni_{0.05}Mg_{0.925}O$, (b) $Mo_{0.05}Ni_{0.05}Mg_{0.9}O$, (c) $Mo_{0.1}Ni_{0.05}Mg_{0.85}O$, (d) $Mo_{0.2}Ni_{0.05}Mg_{0.75}O$, and (e) $Mo_{0.4}Ni_{0.05}Mg_{0.55}O$.

measurements, the purity of CNTs was always higher for the carbon deposit synthesized with the longer reaction time of 8 h than for that synthesized for 1 h, strongly suggesting that the impurities are not carbonaceous but are due to the catalysts used for the synthesis. As shown in Figure 6, it was found that thin carbon nanotubes are produced for all the catalysts used. However, the outer diameter and the thickness apparently increased with increasing Mo mole fractions. For the $Mo_{0.025}Ni_{0.05}Mg_{0.925}O$ catalyst, the number of graphene layers was only 2−3, and distribution was relatively uniform. On the other hand, above a Mo fraction of 0.1, the CNTs became thick and the distribution of the thickness was not as uniform.

We thus analyzed the dependence of thickness and diameter of CNTs on the catalyst composition for the $Mo_xNi_{0.05}Mg_{0.95-x}O$ catalyst series with different Mo contents, using TEM. Figure 7 shows the distribution of the inner diameters, outer diameters, and the number of graphene layers. It can be seen that the inner diameters of the CNTs do not differ much, regardless of the Mo mole fraction, while the outer diameters and the numbers of layers increase with increasing Mo mole fraction. At the lower Mo mole fraction of 0.025, the inner and outer diameters ranged from 1.5 to 3.8 nm and from 3.0 to 7.6 nm, respectively, with relatively narrow peaks. At the higher Mo mole fractions, the distributions of the diameters as well as the thickness became broad. The variation in the diameter is ascribed to the catalyst particle size, as described later. Here, it should be pointed out that 2−3-walled CNTs have been selectively produced (more than 60%) by the decomposition of CH_4 over the $Mo_{0.025}Ni_{0.05}Mg_{0.925}O$ catalyst. That is, this catalyst is effective for the synthesis of double-walled CNTs.

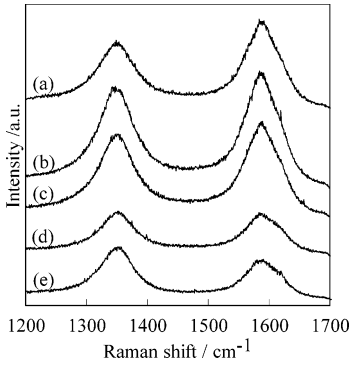

Figure 8. Raman spectra of carbon nanotubes produced in 8 h: (a) $Mo_{0.025}Ni_{0.05}Mg_{0.925}O$, (b) $Mo_{0.035}Ni_{0.05}Mg_{0.915}O$, (c) $Mo_{0.05}Ni_{0.05}Mg_{0.90}O$, (d) $Mo_{0.1}Ni_{0.05}Mg_{0.85}O$, and (e) $Mo_{0.4}Ni_{0.05}Mg_{0.55}O$.

3.2.2. Raman Spectra of CNTs. Figures 8 and 9 show the Raman spectra of as-grown CNTs obtained over samples of $Mo_xNi_{0.05}Mg_{0.95-x}$ with different Mo mole fractions ranging from 0.01 to 0.6 at 1073 K for 8 h and 1 h, respectively. All of these spectra show two broad bands at 1360 cm^{-1} (D-band) and 1582 cm^{-1} (G-band). The D-band is associated with the vibrations of carbon atoms with dangling bonds in plane terminations of disordered graphite or glassy carbons. The G-band corresponds to the E_{2g} mode of graphite and is related to the vibration of sp^2-bonded carbon atoms in the two-dimensional hexagonal lattice of the graphite layer.[11] In general, the G-band represents the degree of crystallinity in the graphite structure, while the intensity of the D-band indicates the defects, impurities, or lattice

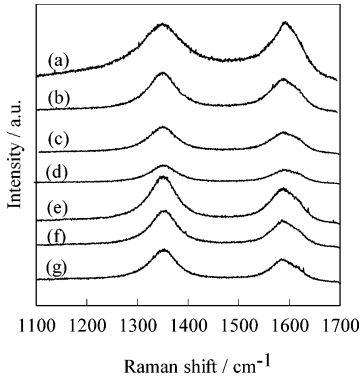

Figure 9. Raman spectra of carbon nanotubes produced in 1 h: (a) $Mo_{0.01}Ni_{0.05}Mg_{0.94}O$, (b) $Mo_{0.035}Ni_{0.05}Mg_{0.915}O$, (c) $Mo_{0.05}Ni_{0.05}Mg_{0.90}O$, (d) $Mo_{0.1}Ni_{0.05}Mg_{0.85}O$, (e) $Mo_{0.2}Ni_{0.05}Mg_{0.75}O$, (f) $Mo_{0.4}Ni_{0.05}Mg_{0.55}O$, and (g) $Mo_{0.6}Ni_{0.05}Mg_{0.35}O$.

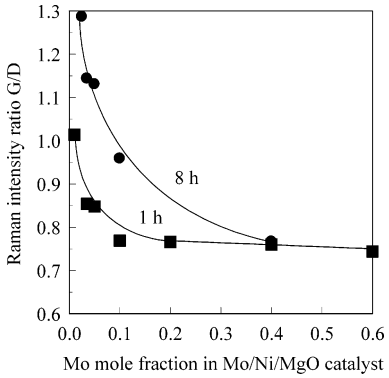

Figure 10. Relationship between I_G/I_D of Raman peaks and the Mo mole fraction for 1 and 8 h reaction times.

distortions in the carbon nanotubes. The results shown in Figures 8 and 9 indicate that the intensity of the G-band decreased while that of the D-band increased upon increasing the Mo mole fraction from 0.025 to 0.4. The relationship between the I_G/I_D intensity ratio and the Mo mole fraction is plotted in Figure 10. The relative intensity of the G-band to the D-band decreased with an increasing Mo mole fraction, indicating more defects in the as-synthesized CNTs. This is consistent with the TEM results mentioned above. This behavior has been observed for the CNT growth with Mo/Co/MgO catalysts,[4] which produced thicker MWNTs at higher Mo fractions.

3.3. Characterization of Catalyst: *3.3.1. TEM Observation of Catalyst.* As described above, the carbon yield and thickness of CNTs vary as a function of Mo or Ni mole fractions. We thus characterized $Mo_xNi_{0.05}Mg_{0.95-x}$ catalysts with different Mo mole fractions (x) by TEM in order to reveal the effect of the catalyst composition on the catalyst structure. Figure 11 shows typical TEM images of reduced catalysts with x values of 0.025, 0.05, 0.1, and 0.4 in $Mo_xNi_{0.05}Mg_{0.95-x}$. We always observed dark spherical particles distributed on bright cubic crystals, where the number of the dark spheres increased with increasing Mo fraction. It is well-known that MgO catalysts have a cubic structure.[12] The dark and bright particles are thus attributed to metal particles consisting of Mo or Ni and to MgO crystals, respectively. The metallic particles are mainly found on the MgO cubes for the catalysts with less Mo, but large metal particles 15 nm or larger in diameter are present and distributed without being supported on MgO in $Mo_{0.4}Ni_{0.05}Mg_{0.55}O$. The average size of MgO microcrystals was estimated to be 15∼20 nm from the TEM images, and this size tended to decrease with increasing Mo mole fraction.

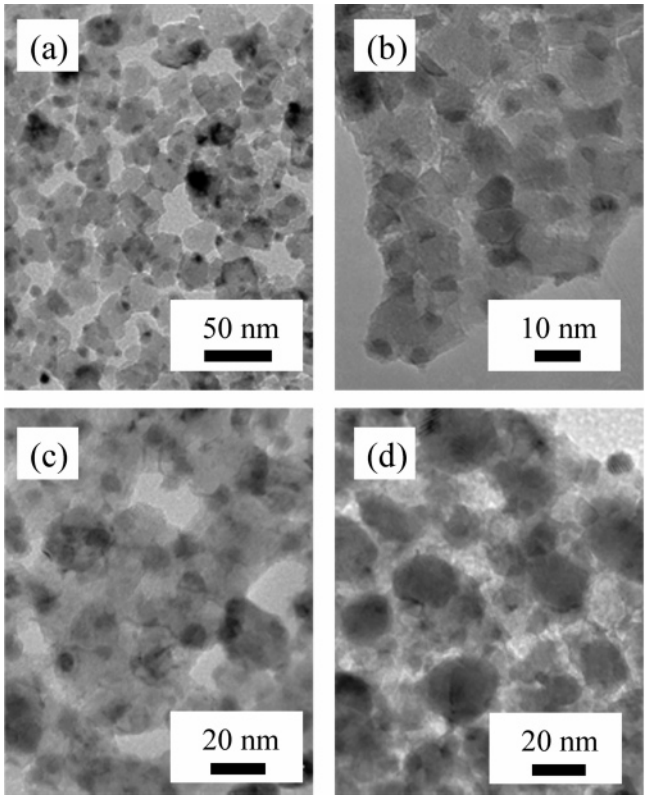

Figure 11. TEM images of catalysts after reduction at 923 K for 1 h: (a) $Mo_{0.025}Ni_{0.05}Mg_{0.925}$, (b) $Mo_{0.05}Ni_{0.05}Mg_{0.9}$, (c) $Mo_{0.1}Ni_{0.05}Mg_{0.85}$, and (d) $Mo_{0.4}Ni_{0.05}Mg_{0.55}$.

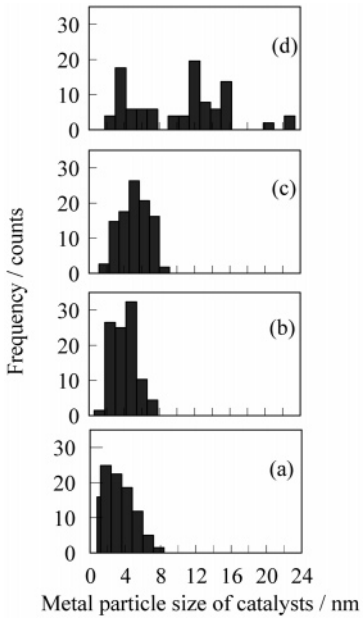

Figure 12. Metal particle size distribution histogram for catalysts: (a) $Mo_{0.025}Ni_{0.05}Mg_{0.925}O$, (b) $Mo_{0.05}Ni_{0.05}Mg_{0.90}O$, (c) $Mo_{0.1}Ni_{0.05}Mg_{0.85}O$, and (d) $Mo_{0.4}Ni_{0.05}Mg_{0.55}O$.

On the other hand, the sizes of the metal particles increased with increasing Mo mole fraction. As shown in Figure 11d, large particles are seen at a Mo mole fraction of 0.4. We thus examined the distribution of metal particle sizes for catalysts with different Mo mole fractions by measuring the sizes and counting these particles in the TEM images. Figure 12 shows the particle size distribution for the reduced catalyst with x values of 0.025, 0.05, 0.1, and 0.4. At the small Mo mole fraction of 0.025, the particle size was in the range of 1.5−6

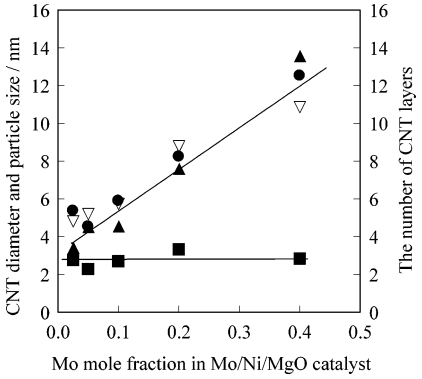

Figure 13. Average sizes of CNTs and metal vs Mo mole fraction in $Mo_xNi_{0.05}Mg_{0.95-x}O$ catalyst: (■) inner diameter of CNTs, (●) outer diameter of CNTs, (▲) layers of CNTs, and (▽) metal particle size.

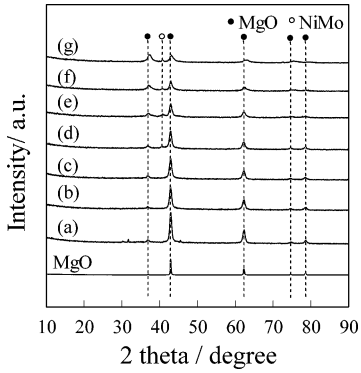

Figure 14. XRD patterns of catalysts after reduction at 923 K for 1 h: (a) $Ni_{0.05}Mg_{0.95}O$, (b) $Mo_{0.025}Ni_{0.05}Mg_{0.925}O$, (c) $Mo_{0.05}Ni_{0.05}Mg_{0.9}O$, (d) $Mo_{0.1}Ni_{0.05}Mg_{0.85}O$, (e) $Mo_{0.2}Ni_{0.05}Mg_{0.75}O$, (f) $Mo_{0.4}Ni_{0.05}Mg_{0.55}O$, and (g) $Mo_{0.6}Ni_{0.05}Mg_{0.35}O$.

nm. The size distribution became larger with increasing Mo mole fraction, and the distribution became broad. In particular, at a Mo mole fraction of 0.4, the distribution was very broad and seemed to be separated into two parts, that is, small particles of 2−8 nm and larger ones over 8 nm. The large particles 8 nm or larger in diameter are considered to be due to sintered particles that cannot be supported on the MgO cubes. The results shown here clearly indicate that low Mo and Ni contents are necessary for keeping the metal particles small.

It should be noted that the distribution features seen in Figure 12 change significantly around $x = 0.4$ (total mole fraction of 0.45), which is the critical point as described in the results for the carbon yield (3.1.1). Below $x = 0.4$, the distribution appears sharp and the particle size is as small as 2−8 nm. On the other hand, above $x = 0.3-0.4$, the distribution becomes broader and larger particles with diameters over 15 nm appear; this is comparable to the size of MgO (15−20 nm). This indicates that metal particles larger than MgO cannot be supported on MgO. Furthermore, the number of supported metal particles should decrease at higher Mo mole fractions because the relative amount of MgO is decreased. In other words, the number of unsupported large particles should increase at higher metal mole fractions. It is considered that the larger particles show little catalytic activity for CNT synthesis, on the basis of the results showing a smaller carbon yield at lower MgO contents, as shown in Figures 1−3. Accordingly, the role of MgO is to stabilize metal particles smaller than MgO itself and to prevent them from sintering at high reaction temperatures, as only the small supported particles act as a catalyst for CNT synthesis.

We analyzed TEM images of the CNTs and catalysts in order to examine the correlation between particle size and CNT size, that is, inner diameter, outer diameter, and thickness of CNTs. The average sizes of CNTs and catalyst are shown as a function of the Mo mole fraction in Figure 13, to show this feature more clearly. The inner diameter of CNTs was consistently found to be 2−3 nm, even at higher Mo mole fractions, while the outer diameter, the number of layers of graphene sheets, and the metal particle sizes increased with increasing Mo content. The average number of graphene layer ranges from 3 to 14. Interestingly, the outer diameter ranging from 3 to 13 nm is comparable to the metal particle size, meaning that the metal particle sizes determine the outer diameters of the CNTs. This further indicates that the outer diameter has a memory for the size of reduced metal catalysts. It is thus concluded that the average of the outer diameters of 3−13 nm and the thicknesses of 2−14 layers can be controlled by the Mo fraction, while keeping the inner diameter at 2−3 nm. It was not possible to analyze the TEM images of catalysts with mole fractions of Mo or Ni above 0.4.

3.3.2. XRD of Catalyst. The bulk crystal structures of catalysts and their sizes before and after the CNT synthesis were then examined by XRD. Figure 14 shows the XRD patterns of reduced catalysts $Ni_{0.05}Mg_{0.95}O$, $Mo_{0.025}Ni_{0.05}Mg_{0.925}O$, $Mo_{0.05}Ni_{0.05}Mg_{0.9}O$, $Mo_{0.1}Ni_{0.05}Mg_{0.85}O$, $Mo_{0.2}Ni_{0.05}Mg_{0.75}O$, $Mo_{0.4}Ni_{0.05}Mg_{0.55}O$, and $Mo_{0.6}Ni_{0.05}Mg_{0.35}O$ (a−g, respectively). The diffraction peaks of the catalysts with Ni or Mo mole fractions below 0.05 are basically identical to that of pure MgO, meaning that the Mg included in the catalysts is present as crystalline MgO and that Ni and Mo particles are too small to show their diffraction peaks, which is in agreement with the TEM results. Here, the Mo and Ni should be reduced by hydrogen to metal because these catalysts were reduced at a high temperature of 923 K. For the catalysts with Mo mole fractions over 0.1, a new peak appeared at $2\theta \approx 40.95°$ for a Mo mole fraction of 0.2 or greater, as shown in Figure 14. This peak is attributed to the Mo−Ni alloy because the pure Mo peak[13] is known to appear at $2\theta = 40.5°$ and because Mo−Ni alloy peaks are known to appear at 40.67−40.95° at higher Mo contents, that is, Mo-rich Mo−Ni alloy.[14] Moreover, these new peaks shift to a lower 2θ and become larger upon increasing the Mo content from 0.1 to 0.6. Note that, below the critical point of 0.4, the Mo−Ni alloy peak is observed for $Mo_{0.1}Ni_{0.05}Mg_{0.85}$ and $Mo_{0.2}Ni_{0.05}Mg_{0.75}$. This indicates that Mo−Ni alloy particles were formed during the reduction of the catalysts with hydrogen.

The peak at 37.2° increased even with a decreasing Mg fraction. This can be explained by the growth of the peak for the face-centered cubic (fcc) Mo particles.[15] The Mo bulk has a body-centered cubic (bcc) structure, but nano Mo particles with a fcc structure have been predicted theoretically[16] and observed by XRD.[15,17]

The intensity of the MgO peak in Figure 14 decreased and the peak became broader with increasing Mo mole fraction. The size of the MgO was estimated from the width of the MgO [200] peak. The average size of MgO was found to decrease from 18.3 to 14.5 nm upon increasing the metal components (Ni or Mo). The size estimated from the XRD measurements is in good agreement with that determined by TEM as described in section 3.3.1.

In comparison, another series of the catalysts that had a fixed Mo mole fraction of 0.1, that is, $Mo_{0.1}Ni_xMg_{0.9-x}O$ ($x = 0.1-0.8$), was characterized by XRD after reduction of the catalysts, as shown in Figure 15. A diffraction pattern of pure Ni is also seen here. Again, the catalysts with Ni contents below 0.05 gave no Mo or Ni peak, indicating that metal particles consisting of Mo and Ni were well-dispersed and small. The XRD patterns show notable changes when the Ni mole fraction reaches 0.1

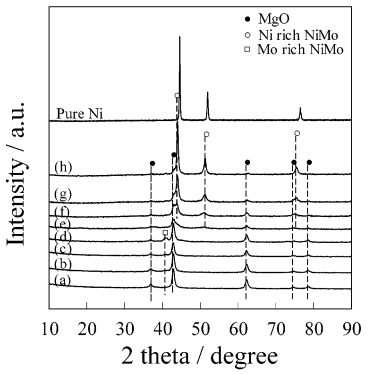

Figure 15. XRD patterns of $Mo_{0.1}Ni_xMg_{0.9-x}O$ ($x = 0.1-0.8$) catalysts after reduction at 923 K for 1 h: (a) $Mo_{0.1}Ni_{0.01}Mg_{0.89}O$, (b) $Mo_{0.1}Ni_{0.025}Mg_{0.875}O$, (c) $Mo_{0.1}Ni_{0.05}Mg_{0.85}O$, (d) $Mo_{0.1}Ni_{0.1}Mg_{0.8}O$, (e) $Mo_{0.1}Ni_{0.2}Mg_{0.7}O$, (f) $Mo_{0.1}Ni_{0.4}Mg_{0.5}O$, (g) $Mo_{0.1}Ni_{0.6}Mg_{0.3}O$, and (h) $Mo_{0.1}Ni_{0.8}Mg_{0.1}O$.

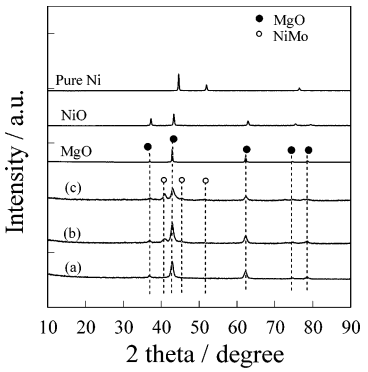

Figure 16. XRD patterns of catalysts after reduction with H_2 at 923 K for 1 h: (a) $Mo_{0.05}Ni_{0.05}Mg_{0.9}$, (b) $Mo_{0.1}Ni_{0.1}Mg_{0.8}$, and (c) $Mo_{0.2}Ni_{0.2}Mg_{0.6}$. The patterns for Ni, NiO, and MgO are also shown.

or more. That is, new diffraction peaks due to Ni−Mo alloys appear at $2\theta = 40.9°$, 43.8°, 50.9°, and 74.9°. Note that the XRD patterns of Mo−Ni alloy differ greatly, depending on the composition.[18] It is known that if the Mo content is small (<20%), $MoNi_3$ or $MoNi_4$ is formed, giving XRD peaks at 43.8°, ~50.9°, ~74.9°, and 89°. On the other hand, the peak of the Mo-rich alloy appears at 40.9° as mentioned above. It is interesting to determine what kind of alloy is formed below the total metal mole fraction of 0.4, at which composition thin CNTs are synthesized by the small catalyst particles. For the $Mo_{0.1}Ni_{0.1}Mg_{0.8}$ and $Mo_{0.1}Ni_{0.2}Mg_{0.7}$ catalysts, Mo-rich and Ni-rich Mo−Ni alloys, respectively, were found to form. It is thus clear that the active catalyst prior to use for the CNT synthesis is composed of Mo−Ni alloys, though different kinds of Mo−Ni alloy are possible.

In Figure 15, it can be seen that, above a total (Ni + Mo) mole fraction of 0.4, intense peaks due to Ni-rich Mo−Ni alloy at 44.4°, 51.2°, and 75.5° grow and are sharpened, indicating that the Ni−Mo alloy particle sizes become much larger at higher Ni contents. This is consistent with the TEM results discussed above. Taking into consideration that the carbon yield decreased greatly at the higher Ni contents, the large alloy particles are inactive as catalysts for the carbon deposition.

We also examined a series of $Mo_xNi_xMg_{1-2x}$ catalysts with a 1:1 Mo/Ni molar ratio in our attempts to prepare a MoNi alloy. The XRD patterns of these reduced catalysts are shown in Figure 16. Although the $Mo_{0.05}Ni_{0.05}Mg_{0.9}$ catalyst exhibited the same XRD pattern as MgO, the $Mo_{0.1}Ni_{0.1}Mg_{0.8}$ and $Mo_{0.2}Ni_{0.2}Mg_{0.8}$ catalysts showed new phases around 40−45°. The XRD peaks at 40.9°, 42.2°, and 45.8° have been assigned by Jakšić et al.[14]

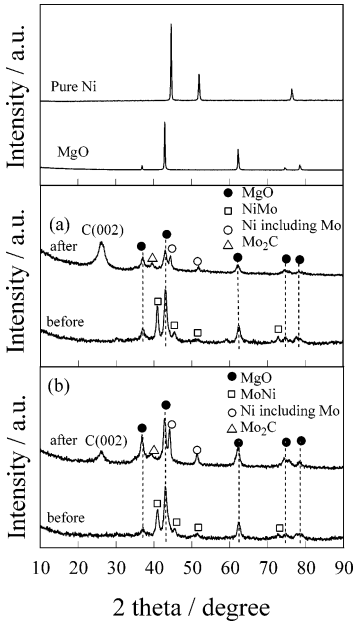

Figure 17. XRD patterns of catalysts after reduction at 923 K for 1 h and after CNT synthesis at 1073 K for 5 min: (a) $Mo_{0.25}Ni_{0.15}Mg_{0.6}O$ and (b) $Mo_{0.2}Ni_{0.2}Mg_{0.6}O$.

as being due to a Mo−Ni alloy with a 1:1 molar ratio. They also prepared several Mo−Ni alloy compounds of MoNi, $MoNi_2$, $MoNi_3$, and $MoNi_4$ by arc melting of the pure components (Ni, Mo) under an argon atmosphere and analyzed the structures of those alloys by XRD. Apart from $MoNi_4$, all the alloys investigated had a multiphase structure. For example, the $MoNi_3$ sample contained Mo and $MoNi_4$ phases in addition to the $MoNi_3$ phase. Moreover, if the Mo/Ni ratio is 50/50, very different XRD patterns appear, in which the MoNi sample contains MoNi and $MoNi_4$ as separated phases. On the basis of the literature, the XRD patterns of $Mo_{0.1}Ni_{0.1}Mg_{0.8}$ and $Mo_{0.2}Ni_{0.2}Mg_{0.8}$ shown in Figure 16 indicate MoNi alloy formation.

The XRD measurements described above were carried out on the catalysts prior to CNT synthesis. To examine the state of the catalysts during CNT synthesis, postreaction catalysts were examined by XRD. Figure 17 shows XRD patterns of $Mo_{0.25}Ni_{0.15}Mg_{0.6}O$ and $Mo_{0.2}Ni_{0.2}Mg_{0.6}O$ catalysts after reduction with H_2 at 923 K for 1 h, as well as those obtained after CNT synthesis at 1073 K for 5 min. Before the CNT synthesis reaction, MoNi alloy and MgO peaks were observed in the XRD patterns for both catalysts. After the reaction, the Ni−Mo alloy peak disappeared and new peaks attributed to Mo_2C and Ni (or a small amount of Mo-including Ni) appeared at $2\theta = 41.0-40.84°$ [19] and at 44.16−44.36° and 51.33−51.80°,[18] respectively. These results indicate conversion of the Mo−Ni alloy particles into two separate phases of Mo_2C and Ni (or Mo-including Ni) during the 8 h of reaction with methane at 1073 K. Figure 18 shows the XRD patterns of the $Mo_xNi_xMg_{1-2x}$ series catalysts after CNT synthesis at 1073 K for only 5 min. The results also show that the Mo_2C and Ni (or Ni including a small amount of Mo) were formed from the Mo−Ni alloy immediately after the CNT synthesis.

The results shown in Figures 17 and 18 indicate that carbon formed on the metal catalyst by decomposition of CH_4 initially dissolved into the bulk of the Mo−Ni alloy particles and carbon and Mo formed a stable Mo_2C compound, leading to the segregation of Ni domains in a single particle. The thermal stability and XRD patterns for Mo_2C and Ni_3C have been reported in the literature. It has been reported that MoC_x formed by the carburization of MoO with C_2H_4 at 973 K is stable at

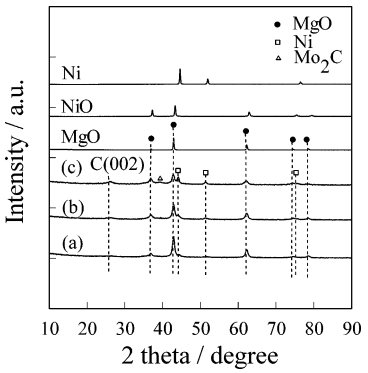

Figure 18. XRD patterns of catalysts after CNT synthesis at 1073 K for 5 min: (a) $Mo_{0.05}Ni_{0.05}Mg_{0.9}O$, (b) $Mo_{0.1}Ni_{0.1}Mg_{0.85}O$, and (c) $Mo_{0.20}Ni_{0.2}Mg_{0.75}O$.

~1273 K.[20] On the other hand, nickel carbide (Ni_3C) decomposes at around 581−823 K,[21] which is lower than the present reaction temperature for the CNT synthesis (1073 K). No XRD peak due to nickel carbide (Ni_3C) was observed at $2\theta = 44.9°$, which is higher than that of pure Ni.[9,22] The amount of carbon soluble in Ni is only 0.1 wt % at 1083 K, so nickel carbide should not form at the reaction temperature used here.[23]

3.4. Proposed Roles of Mo and Ni in CNT Formation. It is clear that Mo and Ni coexist in a single catalyst particle before CNT synthesis because the formation of Mo−Ni alloys was observed in this study. This indicates that the phase separation from the Mo−Ni alloys to Mo_2C carbide and Ni should take place in a single catalyst particle during CNT synthesis. We also found that the physical mixtures of Mo/MgO and Ni/MgO showed little activity for CNT synthesis, indicating that coexistence of Mo_2C and Ni in a single particle is required for the catalytic performance. The excellent catalytic activity of Mo/Ni/MgO compared to that of Mo/MgO and Ni/MgO is thus ascribed to the bifunctional role of the Mo_2C and Ni phases. The metallic Ni allows the dissociation of CH_4, since Ni is a well-known catalyst for CH_4 dissociation[24] and related catalytic reactions such as steam reforming[25] and CO_2 reforming[26] of CH_4.

On the other hand, the role of Mo_2C is ascribed to reserving carbon inside a catalyst particle because, on the basis of the literature, it is suggested that a catalyst for CNT synthesis requires carbon in the bulk of the metal catalyst. That is, Ni (or Co or Fe) catalysts without Mo show catalytic activity for CNT synthesis at lower temperatures, which can be explained by the existence of nickel carbide (cobalt carbide or iron carbide) in the bulk of the catalysts. Ni catalysts are not active for the CNT synthesis at temperatures above 1000 K,[10,27] because carbide is not thermodynamically stable at these higher temperatures. These facts suggest that the presence of carbon in the bulk of the catalyst is a prerequisite for producing CNT on the catalysts, which should then segregate to the catalyst surface to assemble the graphene network. Although the dissociation of CH_4 is an activation process, so that the rate of carbon deposition should increase at higher reaction temperatures, the experimental results have shown that the CNT yield decreased upon increasing the reaction temperatures above 800 K. This is explained by deactivation due to carbonaceous surface without formation of a CNT network. This has already been confirmed by recent preliminary data. We thus consider that if the Mo_2C and Ni phases coexist in a single catalyst particle, penetration and segregation of carbon is possible in the catalyst particle because the carbon can be exchanged with that of Mo_2C.

The prerequisite of the existence of carbon in the bulk of metal catalysts means that the segregation of carbon from the bulk is very important process in CNT synthesis. Helvec et al.[28] have observed, by in situ TEM, that carbon segregates preferentially at the step-edges of Ni catalyst surfaces, leading to CNT formation. We have observed, by scanning tunneling microscopy (STM), that carbon preferentially segregates at step-edges on Ni(111) and stepped Ni(111) surfaces.[29]

4. Summary

Thin MWCNTs were produced by decomposition of CH_4 with Mo/Ni/MgO catalysts in a controlled way with respect to the diameter and thickness of the CNTs. That is, the averages of the outer diameters and the numbers of layers were controlled from 3 to 13 nm and from 2 to 14, respectively, by changing the Mo fractions. The outer diameter correlated well with the size of the metal catalysts including Ni and Mo_2C. On the other hand, the inner diameter was constant at 2−3 nm regardless of the catalyst composition. As regards the yield of CNTs, the optimal mole fraction of MgO was about 0.6, at which small catalyst particles composed of Mo and Ni (3−13 nm) were supported on MgO cubic particles 15−18 nm in size. Decreasing the MgO fraction resulted in a decrease in the size of MgO particles, so that the metal catalyst particles of Mo and Ni could not be supported on the MgO surface. The unsupported Mo and Ni catalysts suffered sintering and were turned into large particles that were inactive for the CNT synthesis. This means that the role of MgO is to support small catalysts consisting of Mo and Ni without sintering, which work as active catalysts for the CNT synthesis. It was found that Mo−Ni alloy particles were formed after reduction with hydrogen prior to the CNT synthesis, indicating the coexistence of Mo and Ni in a single particle on the MgO support. After the CNT synthesis, two phases of Mo_2C and Ni (with a small amount of Mo) were found by XRD, indicating that very stable Mo_2C is formed under the steady-state condition at 1073 K without formation of unstable Ni_3C. The role of Mo_2C is ascribed to keeping carbon in the bulk of the catalyst particles, which enables segregation of the carbon to specific sites on the catalyst surface for assemblage of the graphene sheets.

References and Notes

(1) Iijima, S. *Nature* **1991**, *354*, 56.

(2) (a) Bethune, D. S.; Kiang, C. H.; deVries, M. S.; Gorman, G.; Savoy, R.; Vazquez, J.; Beyers, R. *Nature* **1993**, *363*, 605. (b) Thess, A.; Lee, R.; Nikolaev, P.; Dai, H.; Petit, P.; Robert, J.; Xu, C.; Lee, Y. H.; Kim, S. G.; Rinzler, A. G.; Colbert, D. T.; Scuseria, G. E.; Tomanek, D.; Fisher, J. E.; Smalley, R. E. *Science* **1996**, *273*, 483. (c) Sen, R.; Govindaraj, A.; Rao, C. N. R. *Chem. Phys. Lett.* **1997**, *267*, 276. (d) Terrones, M.; Grobert, N.; Olivares, J.; Zhang, J. P.; Terrones, H.; Kordatos, K.; Hsu, W. K.; Hare, J. P.; Townsend, P. D.; Prassides, K.; Cheetham, A. K.; Kroto, H. W.; Walton, D. R. M. *Nature* **1997**, *388*, 52.

(3) Dai, H.; Rinzler, A. G.; Nikolaev, P.; Thess, A.; Colbert, D. T.; Smalley, R. E.; *Chem. Phys. Lett.* **1996**, *260*, 471.

(4) Tang, S.; Zhong, Z.; Xiong, Z.; Sun, L.; Liu, L.; Lin, J.; Shen, Z. X.; Tan, K. L. *Chem. Phys. Lett.* **2001**, *350*, 19.

(5) Ning, Y.; Zhang, X.; Wang, Y.; Sun, Y.; Shen, L.; Yang, X.; Tendeloo, G. V. *Chem. Phys. Lett.* **2002**, *366*, 555.

(6) Liao, X. Z.; Serquis, A.; Jia, Q. X.; Peterson, D. E.; Zhu, Y. T.; Xu, H. F. *Appl. Phys. Lett.* **2003**, *82*, 2694.

(7) Su, M.; Zheng, B.; Liu, J. *Chem. Phys. Lett.* **2000**, *322*, 321.

(8) Cassell, A. M.; Raymakers, J. A.; Kong, J.; Dai, H. *J. Phys. Chem. B* **1999**, *103*, 6484.

(9) Lyu, S. C.; Liu, B. C.; Lee, T. J.; Liu, Z. Y.; Yang, C. W.; Park, C. Y.; Lee, C. J. *Chem. Commun.* **2003**, 734.

(10) (a) Chen, P.; Zhang, H.-B.; Lin, G.-D.; Hong, Q.; Tsai, K. R. *Carbon* **1997**, *35*, 1495. (b) Soneda, Y.; Duclaux, L.; Béguin, F. *Carbon* **2002**, *40*, 965. (c) Frustrei, F.; Spadaro, L.; Arena, F.; Chuvilin, A. *Carbon* **2002**, *40*, 1063−1070. (d) Hang, J. Y.; Lee, S. H.; Sim, K. S.; Kim, J. W. *Synth. Met.* **2002**, *126*, 81.

(11) Moreno, C. J. M.; Yoshimura, M. *J. Am. Chem. Soc.* **2001**, *123*, 741.
(12) Moodie, A. F.; Warble, C. E. *J. Crystal Growth* **1971**, *10*, 26.
(13) Joint Committee on Powder Diffraction Standards, JCPDS International Center for Diffraction Data, Swarthmore, PA.
(14) Jakšić, J. M.; Vojnović, M. V.; Krstajić, N. V. *Electrochim. Acta* **2000**, *45*, 4151.
(15) Lee, G. H.; Huh, S. H.; Jung, H. I. *J. Mol. Struct.* **1998**, *440*, 141.
(16) Tománek, D.; Mukherjee, S.; Bennemann, K. H. *Phys. Rev. B* **1983**, *28*, 665.
(17) Huh, S. H.; Oh, S. J.; Kim, Y. N.; Lee, G. H. *Rev. Sci. Instrum.* **1999**, *70*, 4366.
(18) Chialvo, M. R. G.; Chialvo, A. C. *J. Electroanal. Chem.* **1998**, *448*, 87.
(19) Xiao, T. C.; York, A. P. E.; Al-Megren, H.; Willams, C. V.; Wang, H. T.; Green, M. L. H. *J. Catal.* **2001**, *202*, 100.
(20) Miyao, T.; Shishikura, I.; Matsuoka, M.; Nagai, M.; Oyama, S. T. *Appl. Catal. A* **1997**, *165*, 419.
(21) (a) Itoh, T.; Sinclair, R. *Mater. Res. Soc. Symp. Proc.* **1994**, *349*, 26. (b) Tokumitsu, K. *Mater. Sci. Forum* **1997**, *235*, 127. (c) Nishitani, S. R.; Ishihara, K. N.; Suzuki, R. O.; Shingu, P. H. *J. Mater. Sci. Lett.* **1985**, *4*, 872. (d) Chun, C. M.; Mumford, J. D.; Ramanarayanan, T. A. *J. Electrochem. Soc.* **2000**, *147*, 3680. (e) Shaikhutdinov, S. K.; Avdeeva, L. B.; Novgorodov, B. N.; Zaikovskii, V. I.; Kochubey, D. I. *Catal. Lett.* **1997**, *47*, 35. (f) Nagakura, S. *J. Phys. Soc. Jpn.* **1957**, *12*, 482. (g) Escoubes-Baggioni, M.; Eyraud, C. *Bull. Soc. Chim. Fr.* **1966**, *4*, 1374. (h) Coad, J. P.; Riviere, J. C. *Surf. Sci.* **1971**, *25*, 609.
(22) (a) Laidani, N.; Calliari, L.; Speranza, G.; Micheli, V.; Galvanetto, E. *Surf. Coatings Technol.* **1998**, *100*−*101*, 116. (b) Sun, X. C.; Dong, X. L. *Mater. Res. Bull.* **2002**, *37*, 991.
(23) Isett, L. C.; Blakely, J. M. *Surf. Sci.* **1976**, *58*, 397.
(24) (a) Egeberg, R. C.; Ullmann, S.; Alstrup, I.; Mullins, C. B.; Chorkendorff, I. *Surf. Sci.* **2002**, *497*, 183−193 and reference therein. (b) Beebe, T. P., Jr.; Goodman, D. W.; Kay, B. D.; Yates, J. T., Jr. *J. Chem. Phys.* **1987**, *87*, 2305.
(25) (a) Hayakawa, T.; Suzuki, S.; Nakamura, J.; Uchijima, T.; Hamakawa, S.; Suzuki, K.; Shishido, T.; Takehira, K. *Appl. Catal. A* **1999**, *183*, 273. (b) Asami, K.; Li, X.; Fujimoto, K.; Koyama, Y.; Sakurama, A.; Kometani, N.; Yonezawa, Y. *Catal. Today* **2003**, *84*, 27.
(26) Takeguchi, T.; Kani, Y.; Yano, T.; Kikuchi, R.; Eguchi, K.; Tsujimoto, K.; Uchida, Y.; Ueno, A.; Omoshiki, K.; Aizawa, M. *J. Power Sources* **2002**, *112*, 588 and reference therein.
(27) Takenaka, S.; Kobayashi, S.; Ogihara, H.; Otsuka, K. *J. Catal*. **2003**, *217*, 79.
(28) Helvec, S.; López-Cartes, C.; Sehested, J.; Hansen, P. L.; Clausen, B. S.; Rostrup-Nielsen, J. R.; Abild-Pedersen; Nørskov, J. K. *Nature* **2004**, *427*, 426.
(29) (a) Nakano, H.; Kawakami, S. Fujitani, T.; Nakamura, J. *Surf. Sci.* **2000**, *454*, 295. (b) Nakano, H.; Ogawa, J.; Hirashima, H., Matsumoto, T.; Nakamura, J. Manuscript in preparation.